https://doi.org/10.5194/egusphere-2023-2440
Preprint. Discussion started: 21 November 2023

The extratropical tropopause inversion layer and its correlation with relative humidity

Daniel Köhler[1,*], Philipp Reutter[1], and Peter Spichtinger[1]

[1]Institute for Atmospheric Physics, Johannes Gutenberg University Mainz, Mainz, Germany
[*]now at University of Helsinki, Helsinki, Finland

Correspondence: Philipp Reutter (preutter@uni-mainz.de)

Abstract. This study investigates the influence of relative humidity with respect to ice on the extratropical tropopause inversion layer (TIL). Initially, measurements from radiosondes at a location in Germany were compared with the ERA5 reanalysis data from the ECMWF at the same geographic location. A high level of agreement was observed, with the expected limitation that ERA5 cannot resolve sharp changes in variables like humidity and stability at the tropopause as finely.

When examining the TIL with respect to mean relative humidity over ice in the upper troposphere, a clear relationship with stability becomes evident. Moister profiles, on average, exhibit significantly higher maximum values of the Brunt-Väisälä frequency N^2, indicating a more stable stratification of the tropopause in these cases. This result holds true in both radiosonde measurements and ERA5 data. Considering the thickness of the TIL layer, an inverse pattern emerges. In this case, moister and more stable TILs exhibit a lower thickness.

The strong agreement between radiosondes and ERA5 allows for geographical and seasonal analyses using ERA5 data alone. These analyses reveal consistent relationships in various extratropical regions of the Northern Hemisphere under different meteorological conditions. Differences in the strength of the dependence of TIL properties on relative humidity over ice are evident.

1 Introduction

The Earth's atmosphere, a dynamic and complex multiscale system, plays a pivotal role in regulating our planet's climate and weather patterns. Within this intricate atmospheric structure lies the troposphere, the layer closest to the Earth's surface and the site of most of our planet's weather phenomena. At its upper boundary to the adjacent stratosphere, the troposphere encounters a distinct and intriguing feature known as the tropopause inversion layer (TIL). Birner et al. (2002) introduced the investigation of the TIL using high-resolution radiosonde profiles. Their approach involved employing a tropopause-centered averaging method, where they utilized the thermal tropopause as the reference point for the vertical coordinate instead of sea level.

Situated at the interface between the troposphere and the stratosphere, the TIL represents a unique and enigmatic region characterized by an abrupt increase in temperature with altitude — a significant departure from the typical decrease in temper-

https://doi.org/10.5194/egusphere-2023-2440
Preprint. Discussion started: 21 November 2023

ature observed throughout the lower atmosphere. Thus, a sharp TIL constitutes a strong transport barrier for trace gases and other inert substances.

Since its discovery, a couple of hypothesis were developed to explain the origin and formation of the TIL. Wirth and Szabo (2007) showed in model analysis that baroclinic waves lead to a net sharpening of the tropopause, which leads to stronger TIL. More precisely, an anticyclonic circulation produces a stronger TIL, whereas a cyclonic circulation tends to decrease the strength of the TIL. Gettelman and Wang (2015) and Randel et al. (2007) provided further evidence to support the impact of baroclinic waves on the TIL. Additionally, Randel et al. (2007) suggested a radiative forcing mechanism, where the interaction of ozone and water vapour with radiation are contributing to the TIL formation and persistence. The calculations of Kunz et al. (2009) and the observations of Hegglin et al. (2009) suggest that the radiative forcing mechanism is a dominant effect for the formation and evolution of the TIL.

To investigate the latter mechanism further, we examine the correlation between the relative humidity with respect to ice (RHi), a measure for water vapor in the UTLS region, and the TIL. For this purpose, nearly 10,000 high-resolution radiosonde ascents from a weather station in Germany are analyzed. Additionally, this investigation is combined with the ERA5 reanalysis data from the European Centre for Medium-Range Weather Forecasts (ECMWF) for the same location. This approach allows for an evaluation of the quality of ERA5 data concerning the TIL at the presented German location. Given that the TIL is associated with strong gradients in stability, the comparison of model data with high-resolution measurements is indispensable.

Upon successful assessment of data quality, we can extend our analysis to examine the TIL in a similar manner at other locations. We have focused on regions at a similar geographical latitude but with varying frequencies of baroclinic activity. This approach enables us not only to unravel seasonal differences but also to incorporate the influence of regional peculiarities into the interpretation of the results.

This study is organized as follows. In Section 2 we present details on the data and methods used to identify the important quantities of TIL characteristics. Section 3 presents the results. First a comparison of measurements and reanalysis data is provided, followed by an investigation of the influence of the relative humidity on TIL properties. Finally, we extend the examination on geographical and seasonal variations. Conclusions are found in section 4.

2 Data and Methods

In this section we describe the data sets and the methods for the statistical investigations.

2.1 Data

This study is partly based on radiosonde data from a measurement site at Idar-Oberstein (Germany). This site was selected, because the German weather service (Deutscher Wetterdienst, DWD) provides 9 years of high resolution radiosondes data as open access. The exact used time frame spans from the 1st of January 2011 to the 31th of December 2019.

https://doi.org/10.5194/egusphere-2023-2440
Preprint. Discussion started: 21 November 2023

The radiosonde measurements are compared with the reanalysis data set ERA5 (Hersbach et al., 2020) provided by the ECMWF. After the comparison and evaluation of the data at the selected site, profiles at different geographical locations are investigated based on the ERA5 data set.

2.1.1 Radiosonde data

Idar-Oberstein is one out of 12 stations in Germany, where the DWD executes synoptic (daily at 00, 06, 12, 18 UTC) high resolution radiosondes soundings. The station is located at 49.69° N and 7.33° E at 376 m altitude above sea level.

For the radiosonde measurements the Vaisala RS92-SGP (01/01/2011 - 12/03/2017 & 15/06/2017 - 31/12/2019) sonde and the Vaisala RS41-SGP (28/03/2017 - 14/06/2017) sonde are used, respectively. The characteristics of the two types of radiosondes are very similar, the RS41-SGP has a slightly higher precision than the RS92-SGB (Vaisala, 2014). Therefore, the data is treated as if the entire data set is measured by the RS92-SGP radiosonde.

During one ascent of the radiosonde, the meteorological variables are measured with a time resolution of 0.5 Hertz, providing the longitude & latitude by a GPS-sensor, the geopotential height Φ_g (m), the ambient pressure p (hPa), the temperature T (K) and the relative humidity over liquid water RH (%), respectively. In a first approximation geopotential height Φ_g is equal to the vertical height z. For the considered data set this approximation is quite good, because of Idar-Oberstein's latitude of 49.69° N and the altitude of the measurements never exceed 20 km.

This investigation focus on the upper troposphere and lower stratosphere (UTLS). For obtaining a complete and consistent data set, profiles with a maximum height lower than 20 km and profiles containing missing data are discarded. Over the period from 01/01/2011 to 31/12/2019, the data set contains 10224 single profiles. 419 profiles are discarded, 311 due to insufficient maximum height, 19 due to missing data and 89 due to unscientific temperature ($> 500\,\mathrm{K}$) and relative humidity ($> 300\,\%$).

The uncertainties of the RS92-SGP regarding the measurements are given by the manufacturer (Vaisala, 2013). The temperature sensor has a reaction time less than 2.5 seconds and a total uncertainty of $0.5°C$. The humidity sensor has a response time between 0.5 s and 20 s with a total uncertainty of $\mathrm{RH} = 5\,\%$. The pressure sensor has a total uncertainty of $1\,\mathrm{hPa}$ for 1080 to $100\,\mathrm{hPa}$ and $0.6\,\mathrm{hPa}$ for 100 to $3\,\mathrm{hPa}$.

The radiosonde humidity data are time-lag corrected according to Miloshevich et al. (2004) and the water vapor measurements are corrected using the algorithm and coefficients used by Miloshevich et al. (2009).

2.1.2 ERA5

ERA5 is the latest reanalysis product of the ECMWF (Hersbach et al., 2020). The reanalysis is a mix of a past model forecast and assimilated measurements made at the forecast time. The high resolution data set has a horizontal resolution 0.25° in longitude and latitude. The vertical dimension of the atmosphere is calculated on hybrid sigma/pressure (model) levels in ERA5 (ECMWF, 2020), the number of levels is 137 of which only levels up to the lower stratosphere are used.

For the comparison with the radiosonde data we obtained pseudo-radiosonde profiles, i.e. a vertical column at the fixed grid point. The vertical column is extracted at the closest grid point of the model to 49.75° N and 7.25° E, which will be compared to the radiosondes data set. The date and the time of the extracted columns are matched with the reduced radiosondes data set

https://doi.org/10.5194/egusphere-2023-2440
Preprint. Discussion started: 21 November 2023

to obtain a maximum of comparability between the data set. For comparison, the relevant variables, as, e.g., the geopotential height Φ_p are calculated.

2.1.3 Data gridding

In order to guarantee comparability between the data sets it is mandatory to grid the data sets vertically. A regular grid leads to a consistent spacing between data points, which in in turns allows for a improved statistical analysis. The base of the regular grid is the height z.

Radiosondes use the buoyancy force to ascend, thus the vertical speed and consequently the vertical resolution is not constant. The buoyancy speed of the radiosondes is ranging from $2\,\mathrm{m\,s^{-1}}$ to $8\,\mathrm{m\,s^{-1}}$, returning a vertical resolution of 4 to $16\,\mathrm{m}$, respectively. The final data grid has a $30\,\mathrm{m}$ resolution starting from station height $376\,\mathrm{m}$ above sea level up to $20\,\mathrm{km}$ in order to reduce the amount of unused data. The interpolation is performed with a cubic spline.

The model levels change height with the given atmospheric state, so the geopotential height grid of ERA5 is irregular and inconsistent with respect to time. The data sets is interpolated on the same grid as the radiosondes data ($376\,\mathrm{m}$ to $20\,\mathrm{km}$, with $30\,\mathrm{m}$ resolution) using a cubic spline. The data set is heavily over-sampled with a $30\,\mathrm{m}$ resolution, meaning the high resolution does not provide additional information, but the choice is made in order to make the data set comparable to the radiosonde data.

2.2 Methods

Since most of the desired variables are not directly available, they are calculated from the available information. Therefore, the calculation of the relative humidity with respect to ice RHi (%), the potential temperature θ (K) and the Brunt-Väisälä-frequency N^2 ($\mathrm{s^{-2}}$) are described below.

We choose the variable RHi as a measure for humidity, since this is the thermodynamic control variable for many ice cloud processes, i.e. determining nucleation, growth and evaporation of ice crystals. In addition this humidity variable is a linear variable (in the range between 0 and about 170%), which makes the evaluations simpler and more robust, than using the specific humidity, which in turn does not allow a relation to cloud processes without additional variables. The choice of RHi as a variable is related to the low temperature regime in the UTLS ($T < 240$ K) with hexagonal ice as a stable phase of water.

2.2.1 Calculation of essential variables

The relative humidity is defined as the ratio of the partial pressure of water vapour p_v over the saturation pressure p_s. The saturation pressure is dependent on the phase, i.e. p_s is different between the liquid/gas-boundary compared to the ice/gas-boundary. In this study, the parameterization described by Sonntag (1990) is used for the saturation pressure with respect to liquid water $p_{s,liq}$ and ice $p_{s,ice}$. This choice is motivated by the fact that these formulae are used for radiosonde evaluations. Note, that the most accurate and physically sound formulations for the saturation pressure according to Murphy and Koop

https://doi.org/10.5194/egusphere-2023-2440
Preprint. Discussion started: 21 November 2023

(2005) deviate only slightly from the formulae above in the respective temperature regime. However, for our investigations the deviation is negligible. The quantity RHi is derived from RH of the radiosonde using the following relationship:

$$RHi = RH \cdot \frac{p_{s,liq}}{p_{s,ice}} \tag{1}$$

The ERA5 data set provides the humidity as the specific humidity q ($\mathrm{kg\,kg^{-1}}$) which is converted to the relative humidity over ice using the following approximation:

$$\mathrm{RHi} \approx \frac{q \cdot p}{\epsilon \cdot p_{s,ice}} \tag{2}$$

with the ratio of the molar masses of water and air, $\epsilon = \frac{M_{\mathrm{mol,water}}}{M_{\mathrm{mol,air}}} \approx 0.622$. Potential temperature θ is a quantity in atmospheric sciences, which is equivalent to the specific entropy of dry air, assuming the ideal gas approximation. This quantity allows to compare parcels of air at different pressures levels, and, by definition, it is a conserved quantity for isentropic (i.e. adiabatic) processes. We use the common definition of θ as stated in eq. (3) with a constant specific heat capacity $c_p = 1.005\,\mathrm{kJ\,kg^{-1}\,K^{-1}}$ of dry air:

$$\theta = T \left(\frac{p_0}{p} \right)^{\kappa} \text{ with } \kappa = \frac{R}{c_p} \tag{3}$$

Here, $p_0 = 1000$ hPa denotes the reference pressure level, and $R = 287.05\,\mathrm{J\,kg^{-1}\,K^{-1}}$ is the specific gas constant for air. This definition with constant c_p is accurate enough for investigations in the UTLS (see discussion in Baumgartner et al., 2020).

The static stability or Brunt-Väisälä-frequency squared N^2 is a common measure for the stability of the atmosphere (Hantel, 2013). $N^2 < 0$ characterises an unstable stratification, $N^2 = 0$ a neutral stratification and $N^2 > 0$ a stable stratification. The free troposphere is dominantly stable and the stratosphere is considerably more stable than the troposphere. The static stability is derived from the buoyancy force (i.e. Archimedes' principle) and can be approximate by:

$$N^2 = \frac{g}{\theta} \cdot \frac{\partial \theta}{\partial z} = \frac{g}{T}(\Gamma_d - \Gamma) \tag{4}$$

with $g = 9.8066\,\mathrm{m\,s^{-2}}$ the (mean) gravitational acceleration, Γ_d the dry adiabatic lapse rate and $\Gamma = \frac{\partial T}{\partial z}$ the actual temperature lapse rate, respectively.

This approximation is working under the assumption of dry air and returns on average too high values for the Brunt-Väisälä-frequency (Durran and Klemp, 1982). It is nonetheless used to ensure comparable results with literature which use the dry approximation (Gettelman and Wang, 2015; Birner et al., 2002; Birner, 2006; Erler and Wirth, 2011).

As the measurements of a radiosondes are discrete, a numerical approximation of the derivative is necessary. Since the grid increments are quite small, the numerically derived gradients are highly variable. Thus, a centered approximation of the 4^{th} order is used:

$$\frac{\partial \theta}{\partial z} \approx \frac{4}{3} \frac{\theta_{z+1} - \theta_{z-1}}{z_{z+1} - z_{z-1}} - \frac{1}{3} \frac{\theta_{z+2} - \theta_{z-2}}{z_{z+2} - z_{z-2}} \tag{5}$$

https://doi.org/10.5194/egusphere-2023-2440
Preprint. Discussion started: 21 November 2023

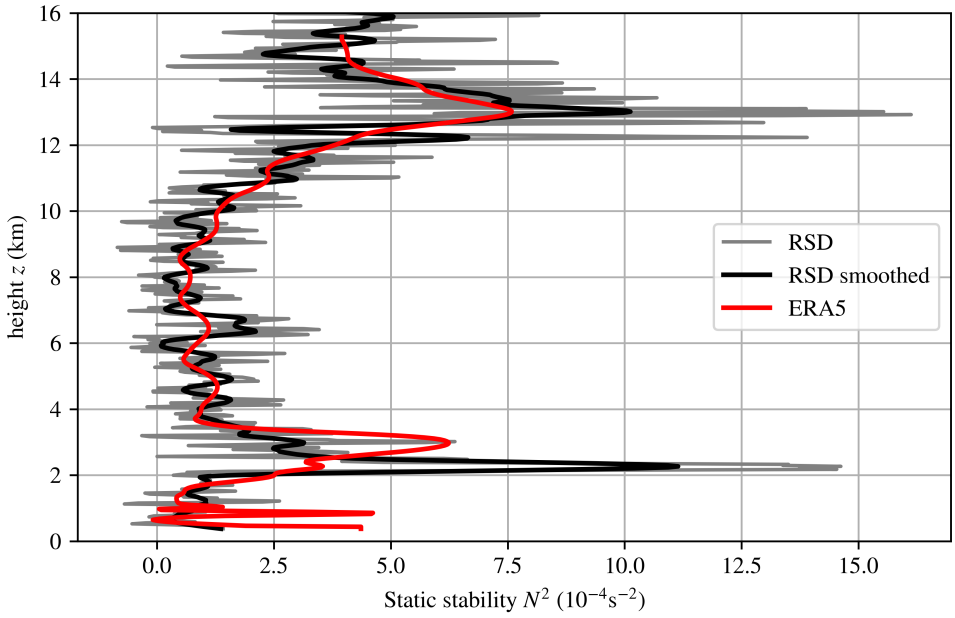

Figure 1. Example of a static stability profile from the 02.01.2011 0 UTC with (grey) the calculated N^2 from radiosonde data, (black) the 330 m window smoothed N^2 from radiosonde data and (red) the calculated N^2 from ERA5 data.

However, even this high order method leads to a highly variable N^2 profile. For a better handling, the profile is additionally smoothed using a running mean with a window of 330 m, as can be seen in Fig. 1.

2.2.2 Calculation of tropopause characteristics

2.2.3 Tropopause height

The tropopause separates the troposphere and the lower stratosphere and is characterised by an inversion of the temperature gradient. One important criterion to define the (thermal) tropopause is the WMO (World Meteorological Organisation) criterion: *"The first tropopause is defined as the lowest level at which the lapse rate decreases to 2 K per kilometer or less, provided also the average lapse rate between this level and all higher levels within 2 kilometers does not exceed 2 K"* (WMO, 1957). Note, that this definition is based on a consideration of large/synoptic scale variations, assuming that the vertical change in the thermodynamic variables (i.e. temperature and pressure, respectively) is smooth enough. However, this is not the case for investigations of high resolution data, as radiosondes or the new generation of reanalysis data (see, e.g., a similar discussion about front detection in Niebler et al., 2022). However, for consistency with former investigations, we adopt this criterion and incorporate this in an algorithm to determine the tropopause height TP_z in both data sets. There are other definitions of the tropopause (e.g. using the potential vorticity for a dynamical tropopause, or the ozone profile for a chemical tropopause); how-

https://doi.org/10.5194/egusphere-2023-2440
Preprint. Discussion started: 21 November 2023

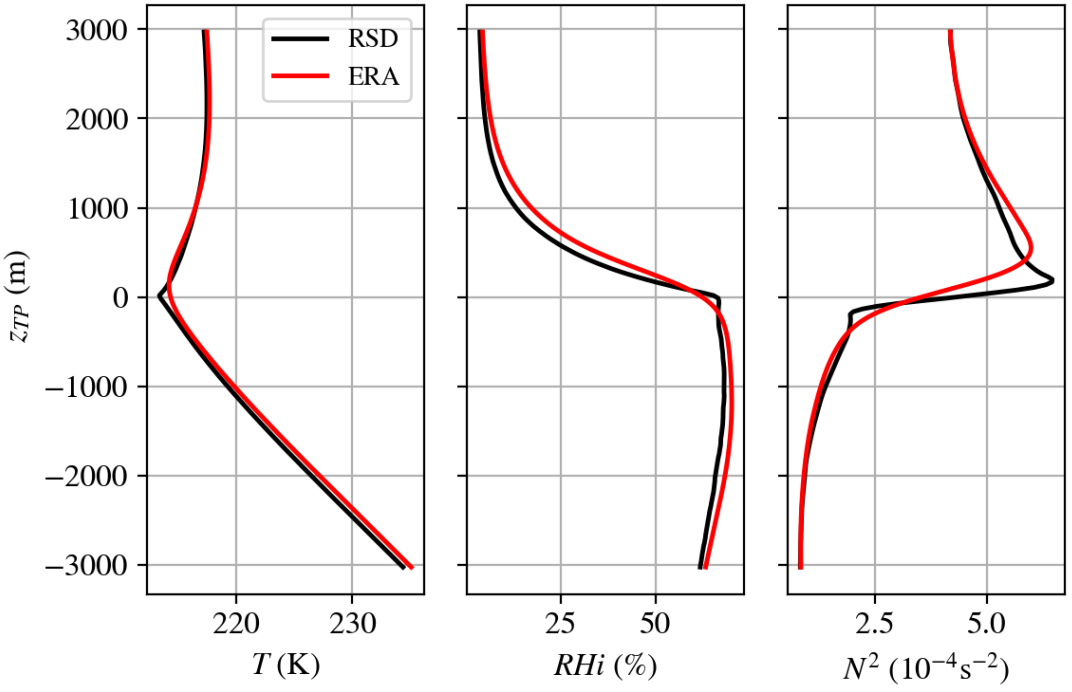

Figure 2. The average vertical profile in the tropopause relative height z_{TP} coordinate system of temperature T, relative humidity over ice RHi and static stability N^2 for the radiosondes (black) and ERA5 (red).

ever, for a better comparison with former investigations (e.g. Birner et al., 2002; Birner, 2006) we use the thermal tropopause, which represents the transport barrier very well. For investigations of the different tropopause definitions we refer to Gettelman et al. (2011).

A tropopause relative height framework is implemented. We introduce a new height variable

$$z_{TP} = z - TP_z \tag{6}$$

relative to the tropopause height TP_z (as derived by the WMO criterion, see above). Negative altitude values z_{TP} denote the upper troposphere, whereas positive altitude values z_{TP} represent the lower stratosphere. For the averaging process the single profiles are transformed into the z_{TP} coordinate system and the arithmetic mean of a meteorological variable $\chi \in \{$temperature, relative humidity, static stability$\}$ is calculated, summing over all profiles at a certain height.

The mean profiles relative to tropopause height of temperature, static stability (N^2), and RHi can be seen in Figure 2 for the radiosonde measurements (black) and the corresponding ERA5 data set (red). Even for the mean profiles the characteristics of the TIL, i.e., the strong increase in N^2 at around TP_z can be seen clearly, as described in the next section.

https://doi.org/10.5194/egusphere-2023-2440
Preprint. Discussion started: 21 November 2023

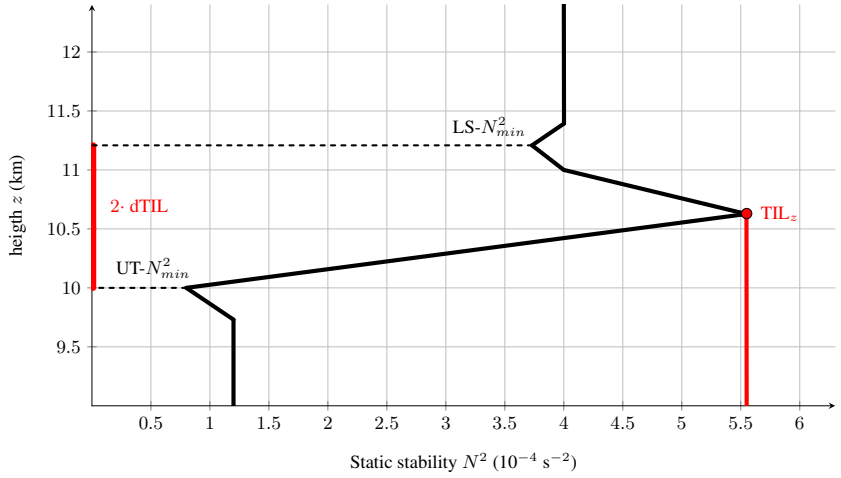

Figure 3. A schematic drawing of the different diagnostics of the tropopause inversion layer, i.e. the TIL depth dTIL and the strength of the TIL, sTIL, respectively.

2.2.4 Tropopause inversion layer

Another important measure in the tropopause region is the tropopause inversion layer (TIL). The TIL is a region of extraordinary high static stability within the tropopause region and was found by averaging vertical profiles with respect to the tropopause level. The TIL is also present in single vertical profiles of radiosondes (Birner et al., 2002) and models (Birner, 2006). The importance of the TIL lies within the diagnostics of upper troposphere and lower stratosphere (UTLS) structures and as a transport barrier for vertical motion (Gettelman et al., 2011).

For this study, we define the TIL strength sTIL as the maximum of the static stability N^2_{max} within 3 km above tropopause level and the altitude level of N^2_{max} as the TIL height TIL$_z$. Two additional heights are defined through two minimum values of N^2: UT-N^2_{min} is the height of the minimum of N^2 in the upper troposphere, and LS-N^2_{min} is the height of the minimum of N^2 within 5 km above TIL height. The TIL depth dTIL is half of the height difference between the UT-N^2_{min} and LS-N^2_{min}. The diagnostic of the TIL are summarized in Figure 3.

In the radiosonde data, the features could not be determined in 126 profiles, which were subsequently discarded as a result. Therefore, the final data set was reduced to 9678 profiles of high resolution radiosonde measurements.

2.2.5 Calculation of humidity measure

The analysis of the humidity of the upper troposphere and the lower stratosphere is based on the average humidity with respect to ice below the TIL, denoted by wRHi. It is calculated by averaging RHi from the height of the 500 hPa pressure surface $p500_z$ up to the TIL level TIL$_z$, as defined in (7).

https://doi.org/10.5194/egusphere-2023-2440
Preprint. Discussion started: 21 November 2023

$$\mathrm{wRHi} = \frac{1}{\mathrm{TIL_z} - p500_z} \int_{p500_z}^{\mathrm{TIL_z}} \mathrm{RHi}(z)\, dz \approx \frac{1}{\mathrm{TIL_z} - p500_z} \sum_{z=p500_z}^{\mathrm{TIL_z}} \mathrm{RHi(z)}\, \Delta z \tag{7}$$

This moisture (or humidity) measure is used in the further course to sort the vertical profiles according to different moisture contents. This quantity is quite robust due to small scale variations, thus representing the overall impact of humidity on the TIL.

3 Results

Based on the spatially and temporally highly resolved ERA5 data, the properties of the tropopause region related to the static stability and relative humidity in this region are investigated in more detail. In a first step, the measured data of the radiosondes are compared with the corresponding data of the reanalysis model. Afterwards, the correlations between moisture and the TIL properties are examined in more detail with the consideration of seasonal and geographical differences.

3.1 TIL properties in measurements and reanalysis data

A very good agreement between the radiosonde measurements and the reanalysis data is the basic prerequisite for further investigations based on the ERA5 data. Therefore, in a first step, the deviations between radiosonde measurements and reanalysis data for the variables temperature T, relative humidity with respect to ice RHi and static stability N^2 are investigated. In the next step, the results for the different heights ($\mathrm{TP_z}$, $\mathrm{TIL_z}$) are investigated. Finally, the TIL properties such as TIL thickness and TIL depth are compared.

3.1.1 Comparision of temperature, relative humidity with respect to ice

The deviation between radiosonde measurements and ERA5 data are quantified by the average measure $\overline{D}(\chi)$ for every single profile. This quantity can be calculated as follows:

$$\overline{D}(\chi) := \frac{1}{z' - z_0} \int_{z_0}^{z'} E(\chi) - R(\chi) \mathrm{d}z \approx \frac{1}{z' - z_0} \sum_{z_0}^{z'} E(\chi(z)) - R(\chi(z)) \Delta z \tag{8}$$

with z_0 the start and z' the end height of the averaging, χ the meteorological variable of interest, E, the ERA5 profile and R the radionsonde profile. Δz is the height difference between two adjacent levels. The resulting data set is visualised in a probability bar chart and the corresponding median, mean and standard deviation for the different variables are presented in figures 4, 5, and 6, respectively.

The temperature deviations between the radiosondes and ERA5 for the upper troposphere (4a) show a Gaussian distribution with a median of $0.027\,\mathrm{K}$ and a mean of $0.034\,\mathrm{K}$ indicating a near symmetric distribution. The mean and median being positive show that the ERA5 reanalysis is slightly warmer than the radiosonde measurements. For the lower stratosphere the distribution

https://doi.org/10.5194/egusphere-2023-2440
Preprint. Discussion started: 21 November 2023

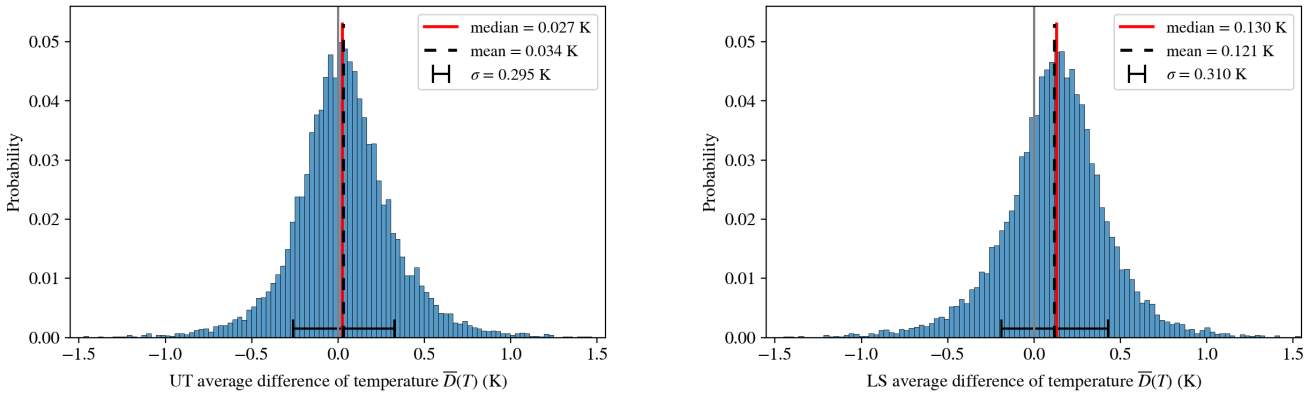

(a) Upper troposphere UT

(b) Lower stratosphere LS

Figure 4. Probability distribution of average difference of temperature $\overline{D}(T)$ between ERA5 and radiosondes for upper troposphere UT (a) and the lower stratosphere LS (b). The median is displayed in red, the mean is represented by a dashed black line and standard deviation σ is represented as error bar. The zero line is denoted as a gray thin line. Positive values mean that ERA5 is warmer than the radiosonde.

of the temperature deviation is similar (4b). However, the median ($0.130\,\mathrm{K}$) and mean ($0.121\,\mathrm{K}$) values are significantly larger. The positive sign again means that ERA5 has on average slightly warmer temperatures compared to the measurements. In order to interepret these results, it should be mentioned that the measurements have an uncertainty of $0.5\,\mathrm{K}$ according to the manufacturer (Vaisala, 2013).

For deriving a robust statement about the humidity impact on the TIL in the tropopause region, the relative humidity with respect to ice (RHi) is used. As mentioned above, this is the key thermodynamic control variable for ice cloud processes, thus determining also the life cycle of ice clouds. The consistency of the moisture data are also important for the description of the average relative humidity with respect to ice wRHi. The distributions in Figure 5 for mean difference show a shift to higher values of RHi in ERA5. This behavior is due to the fact that ERA5 does not capture the moisture gradient at the tropopause as sharply as the radiosonde. In other words, in a thin layer above the tropopause, RHi decreases much faster in the radiosonde data compared to ERA5. This difference dominates the value of $\overline{D}(\chi)$ for each individual vertical profile. The differences are distributed near symmetrically centered around 1.249 % in the upper troposphere and 1.230 % in the lower stratosphere. The standard deviation for the upper troposphere is σ = 10.318 % which is a considerable deviation, where relative humidity over ice ranges from 0% - 105%. In the lower stratosphere, where relative humidity is generally much lower than in the troposphere, the standard deviation is σ = 2.831 %.

The static stability or Brunt-Väisälä-frequency squared N^2 represents the main criteria to identify the tropopause inversion layer and its characteristics. Looking at the probability distribution (Fig. 6), there exists a notable difference between the upper troposphere and the lower stratosphere. In the upper troposphere (Fig. 6a), ERA5 has a tendency to be more stable with a mean = 0.068 $\cdot 10^{-4}$ s^{-2}and a median = 0.058 $\cdot 10^{-4}$ s^{-2}. The distribution is skewed towards smaller average difference values

https://doi.org/10.5194/egusphere-2023-2440
Preprint. Discussion started: 21 November 2023

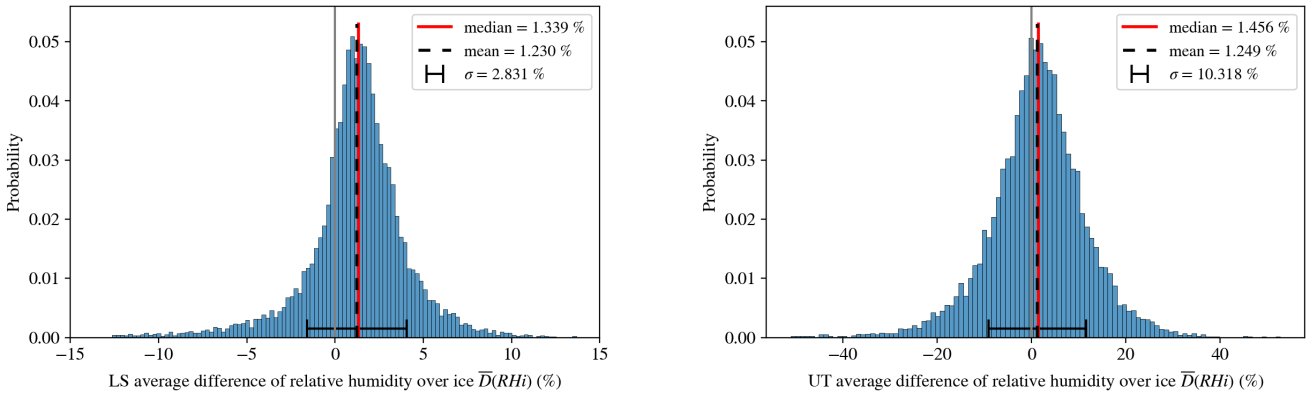

(a) Upper troposphere UT

(b) Lower stratosphere LS

Figure 5. Probability distribution of average difference of relative humidity over ice $\overline{D}(\mathrm{RHi})$ between ERA5 and radiosondes for upper troposphere UT (a) and the lower stratosphere LS. With the median in red, the mean in dashed black and standard deviation σ as error bar. The zero line is denoted as a gray thin line. While the mean difference is small, the spread in the deviation is quite large

of N^2. The majority of the differences lie in the $(0.068 \pm 0.102) \cdot 10^{-4}$ s^{-2} interval. When comparing the average differences to the static stability for the upper troposphere $N^2 = 1.2 \cdot 10^{-4}$ s^{-2} (Hoskins and James, 2014), the static stability is represented well in the ERA5 reanalysis.

In the lower stratosphere (Fig. 6b), ERA5 is more unstable compared to the radiosonde data with a mean = -0.055 $\cdot 10^{-4}$ s^{-2} and a median = -0.046 $\cdot 10^{-4}$ s^{-2} with tendency to smaller absolute values of static stability. The reason for the lower stability in the lower stratosphere in ERA5 is the tropopause inversion layer, which arises through a strong gradient of potential temperature. Due to the lower vertical resolution of ERA5, strong gradients in the variables are less pronounced, leading smaller values of static stability thus resulting in a too unstable vertical profile in the lower stratosphere. Nonetheless, the average difference of -0.055 $\cdot 10^{-4}$ s^{-2} is small compared to the average value of N^2 of 4.0 $\cdot 10^{-4}$ s^{-2}.

3.2 TIL properties and humidity

In the following sections we investigate the relationship between TIL properties and moisture, especially in terms of TIL strength and thickness. As a measure for humidity we use the averaged relative humidity with respect to ice (wRHi) as introduced earlier.

3.2.1 TIL strength and humidity

First, we classify the vertical profiles into tropopause inversion layers of different strengths (sTIL). The classification of sTIL is based on three classes - low sTIL ($\mathrm{sTIL} < 6.8 \cdot 10^{-4}\,\mathrm{s}^{-2}$ for the radiosondes, $\mathrm{sTIL} < 5.2 \cdot 10^{-4}\,\mathrm{s}^{-2}$ for ERA5) , medium sTIL ($6.8 \cdot 10^{-4}\,\mathrm{s}^{-2} < \mathrm{sTIL} < 11.2 \cdot 10^{-4}\,\mathrm{s}^{-2}$ for the radiosondes, $5.2 \cdot 10^{-4}\,\mathrm{s}^{-2} < \mathrm{sTIL} < 8.4 \cdot 10^{-4}\,\mathrm{s}^{-2}$ for ERA5) and

https://doi.org/10.5194/egusphere-2023-2440
Preprint. Discussion started: 21 November 2023

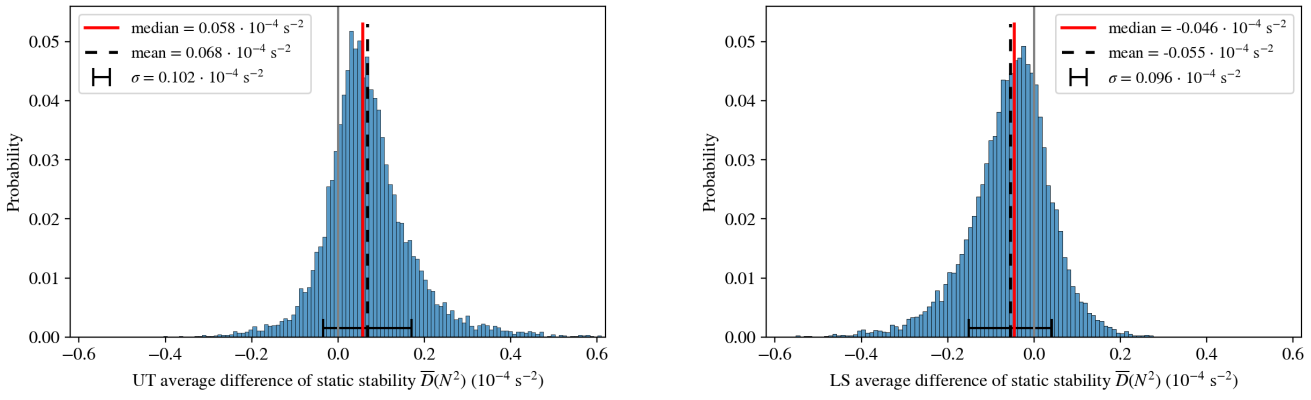

(a) Upper troposphere UT

(b) Lower stratosphere LS

Figure 6. Probability distribution of average difference of static stability $\overline{D}(N^2)$ between ERA5 and radiosondes for upper troposphere UT (a) and the lower stratosphere LS. With the median in red, the mean in dashed black and standard deviation σ as error bar. The zero line is denoted as a gray thin line. The UT is more stable in ERA5 as compared to the radiosonde data, whereas in the LS the ERA5 data indicates smaller values (lower stability) than the radiosonde data.

high sTIL ($11.2 \cdot 10^{-4}\,\mathrm{s}^{-2}$ < sTIL for the radiosondes, $8.4 \cdot 10^{-4}\,\mathrm{s}^{-2}$ < sTIL for ERA5). The classification criteria were chosen such that one third of the vertical profiles fall into each category (low, medium, high). Since the distributions of metrics between ERA5 and radiosondes differ, the exact values of the classification boundaries are also different. Figure 7 shows the corresponding mean profiles for temperature, RHi, and static stability for the radiosondes (left) and the reanalysis data (right).

With the focus on the temperature profile, stronger TILs seem to be correlated with colder temperatures and thus possibly with higher tropopause heights. The correlation between a sharper temperature inversion above the tropopause and a stronger TIL is certainly expected, because the TIL strength is derived from the static stability N^2 which is dependent of the potential temperature gradient and thus the temperature gradients (eq. 4 & 3).

Changing the focus to the correlations of RHi, we find that the TIL is stronger for higher RHi values appearing in the upper tropopause (z_{TP} < 0 m) and right above the tropopause (0 m < z_{TP} < 500 m). In the low sTIL category, the average RHi equals 50 % and is almost constant in the upper tropopause. The medium sTIL category is correlated with an average RHi above 60 % with a slight increase towards the tropopause. The high sTIL category shows average RHi above 70 % with a steep increase towards the tropopause. The increase in relative humidity with respect to ice with increasing height up to the tropopause is a potential indication that vertical motion in the atmosphere is correlated as well to stronger TILs (Wirth and Szabo, 2007), since the resulting adiabatic cooling of air would in turn lead to an increase in RHi.

As expected the ERA5 reanalysis is not able to capture the sharp gradients as well as the high resolution radiosondes. This is noticeable with the sharp kinks in temperature T and relative humidity with respect to ice RHi at tropopause level (z_{TP} = 0 m) and the sharp spikes in the static stability N^2, which are present in the radiosonde data, but are smoothed out in the

https://doi.org/10.5194/egusphere-2023-2440
Preprint. Discussion started: 21 November 2023

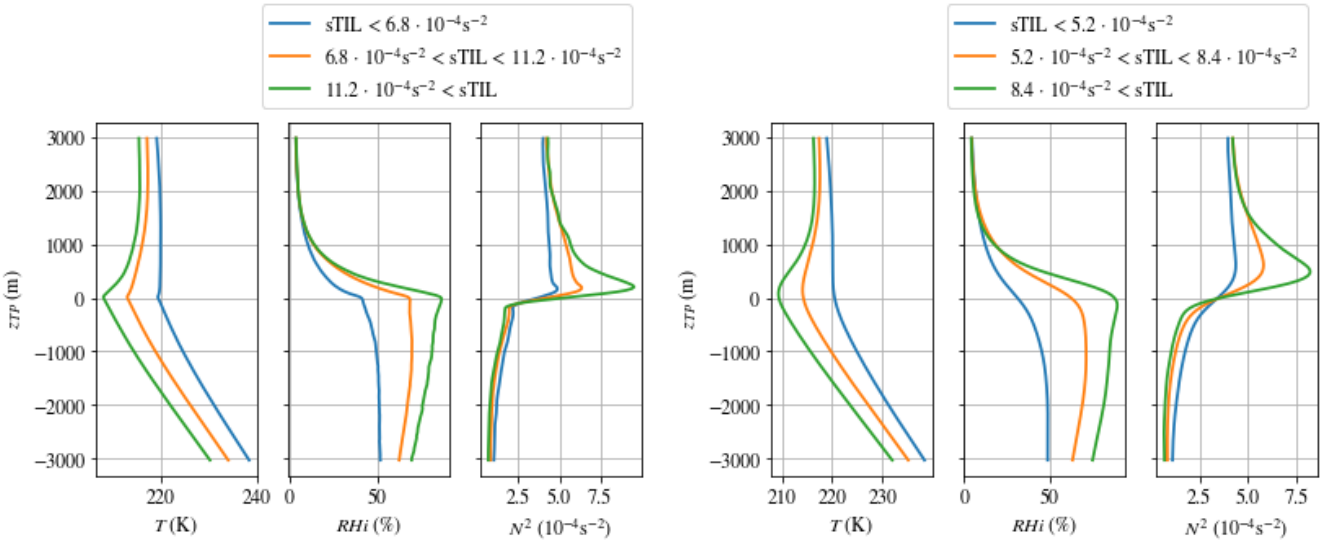

(a) Radiosondes (b) ERA5

Figure 7. The mean vertical profiles of temperature T, relative humidity over ice RHi and static stability N^2 in the tropopause relative height z_{TP}. The mean profiles are classified in terms of tropopause inversion layer strength sTIL. Colors indicate the different sTIL categories. blue: low sTIL value category, orange: medium sTIL value category, green: high sTIL value category. The exact boundary values of the categories are found in the respective legend.

ERA5 data. Despite of these issues related to the resolution of ERA5, the reanalysis data show the same qualitative behaviour for temperature and RHi, respectively. Thus, the ERA5 data set can be used consistently for the investigation of TIL in the extratropics.

Another way to investigate the relationship between humidity and TIL strength is to look at the sTIL distribution as a function of the mean RHi. For this purpose, the sTIL data were divided into three RHi classes: low wRHi (wRHi $\leq$ 45 %), medium wRHi (45 % < wRHi $\leq$ 70 %) and high wRHi (70 % <wRHi), respectively. These distributions are represented in Fig. 8, for radiosonde data (left panel) and ERA5 data (right panel), respectively.

We find that the probability density function (PDF) of the TIL strength is correlated with higher values of wRHi of averaged relative humidity with respect to ice wRHi. This is deducible by the shift of the PDF curve to higher sTIL values with higher wRHi categories. This shift is most obvious at the position of the maximum of the mode of the PDF. The mode for the radiosondes shifts from a maximum at $7.3 \cdot 10^{-4}$ s^{-1} for the low wRHi, to a maximum at $8.2 \cdot 10^{-4}$ s^{-1} for the medium wRHi, and to a maximum at $9.3 \cdot 10^{-4}$ s^{-1} for the high wRHi (Fig. 8a), respectively. We find for ERA5 values from $5.7 \cdot 10^{-4}$ s^{-1} for the low wRHi category, to $6.5 \cdot 10^{-4}$ s^{-1} for the medium wRHi category, and to $7.0 \cdot 10^{-4}$ s^{-1} for the high wRHi category (Fig. 8b), respectively. It is important to mention that the PDF broadens with higher wRHi, which means that the variance of the sTIL values increases. The increased variance does not lead to the different PDF to cross in the left tail of

https://doi.org/10.5194/egusphere-2023-2440
Preprint. Discussion started: 21 November 2023

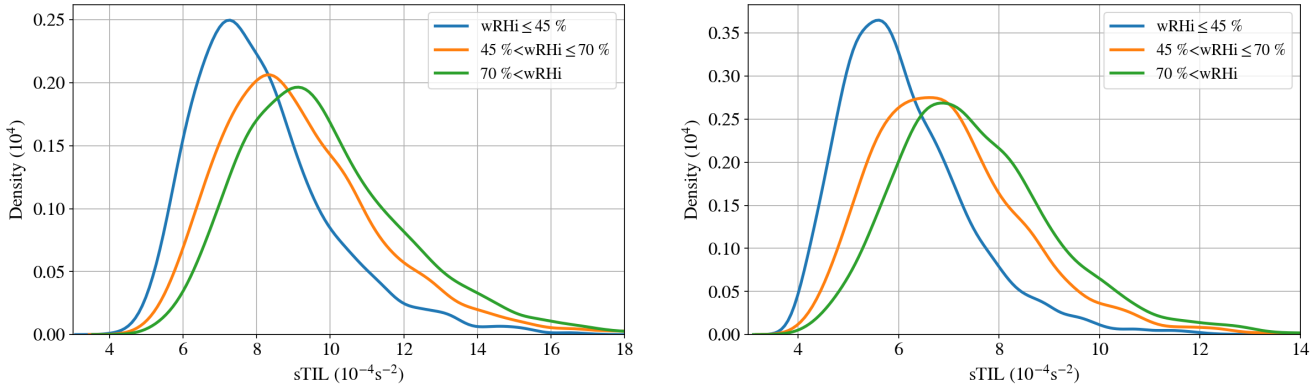

(a) radiosondes (b) ERA5

Figure 8. The probability density function for the radiosondes RSD and ERA5 of the TIL strength sTIL for categories of the average relative humidity over ice wRHi. Colors indicate the different categories with respect to wRHi. blue: low category (wRHi $\leq$ 45 %), orange: medium category (45 % < wRHi $\leq$ 70 %), green: high category (70 % < wRHi).

the function, meaning that weak sTIL always have a higher probability to be in the lower humidity category. Similarly higher sTIL values ($> 9.3 \cdot 10^{-4}$ s^{-1} for radiosondes and $> 6.5 \cdot 10^{-4}$ s^{-1} for ERA5) have a higher probability of being part of the higher wRHi category.

When comparing the radiosondes (Fig. 8a) and ERA5 (Fig. 8b) the similar shape in the probability density and the same trends are apparent, while the values of sTIL are shifted to lower values when comparing ERA5 with the radiosondes.

Again we find the same qualitative behaviour for RS data and reanalysis data, although the quantitative values differ due to the different resolution of the data.

3.2.2 TIL depth and humidity

In addition to the strength of the TIL, the depth of the TIL also shows a correlation with the RHi, which is discussed in this section. We show again pdfs of the TIL depths dTIL distributed into different classes of averaged RHi (Fig. 9). As the average relative humidity over ice wRHi increases, the TIL depth dTIL is shifted to lower values. The total width of the distribution does not change, so the depth of the TIL is always in the range between some few hundreds metres up to about 6000 m. The probability density function shows a formation of a second mode, as found in the ERA5 data set for all wRHi classes (Fig. 9b), as well as in the low wRHi category of the measurements (blue line, Fig. 9a). This formation of a double mode is an artifact of the categorisation process and is thus not of a physical nature. The origin is a fluctuation in the distribution, which is cut off by the boundaries of the categorisation. The artifact makes the interpretation of the mode difficult. Nonetheless there is a correlation between higher dTIL values and lower wRHi values and the variance of the data within each wRHi category is about the same, seen by the similar width and height of the PDF.

https://doi.org/10.5194/egusphere-2023-2440
Preprint. Discussion started: 21 November 2023

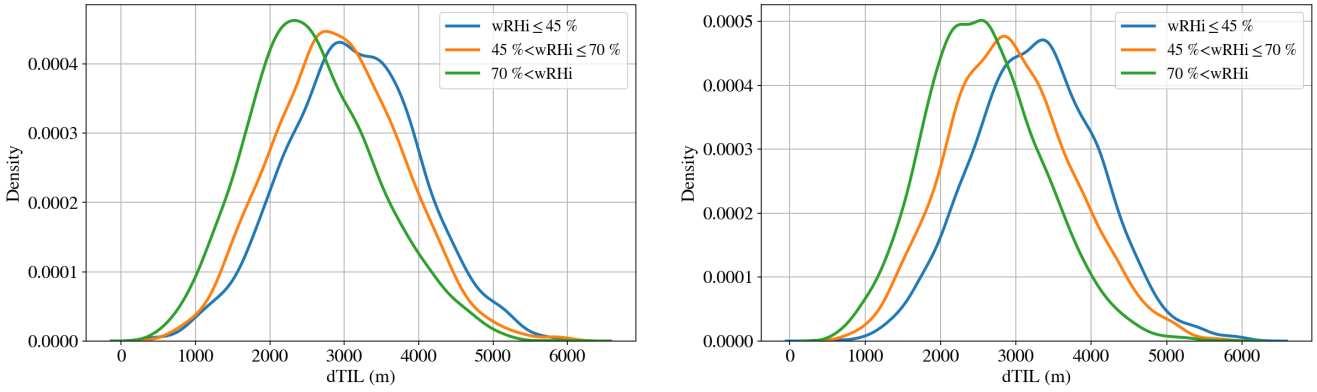

(a) Radiosondes

(b) ERA5

Figure 9. Probability density distribution of the tropopause inversion layer depth dTIL for categories of average relative humidity over ice wRHi. The low category (wRHi $\leq$ 45 %) in blue, the medium category (45 % < wRHi $\leq$ 70 %) in orange and the high category (70 % < wRHi) in green.

In summary, it can be seen that the drier the air is in this region, the thicker the TIL is. Or in other words, a moist upper troposphere is sharpening the TIL in terms of their depth. In combination with the findings from the section before, we can conclude, that for a more humid upper troposphere, we can expect a stronger but vertically more confined TIL feature.

3.3 Geographical variations

We found a correlation between TIL characteristics and humidity for the Idar-Oberstein site in Central Europe with radiosonde measurements and reanalysis data; thus, the next step is to investigate three additional regions in the northern hemisphere at a similar latitude with different meteorological conditions. Here, we address the question whether similar correlations can be found there, although the meteorological situation might be different in terms of large scale dynamics. For this purpose, solely the reanalysis data are now used because of lack of high resolution radiosonde data with acceptable measurement quality for humidity variables.

Idar-Oberstein (Central Europe, C.E., 49.69°N and 7.33°E), which has already been highlighted in detail, has a low cyclone frequency with its maximum in the spring months MAM. The second location is in central Asia (C.A., 49.75°N and 87.25°E) with almost no cyclonic activity throughout the year. The third location is in central USA (USA, 42.50°N and -86.5°E), where the cyclonic frequency for the region is high in winter DJF and spring MAM, and low in summer JJA and autumn SON. The fourth location is in the North Pacific N.P. (49.75°N and -172.75°E), with very high cyclonic frequency through out the year except for a strong minimum in summer (Wernli and Schwierz, 2006).

As already investigated for the Central Europe region (Figure 8), the TIL strength is also distributed into the different moisture classes for the other locations. The results are presented in Figure 10 and confirm that the sTIL values tend to be higher

https://doi.org/10.5194/egusphere-2023-2440
Preprint. Discussion started: 21 November 2023

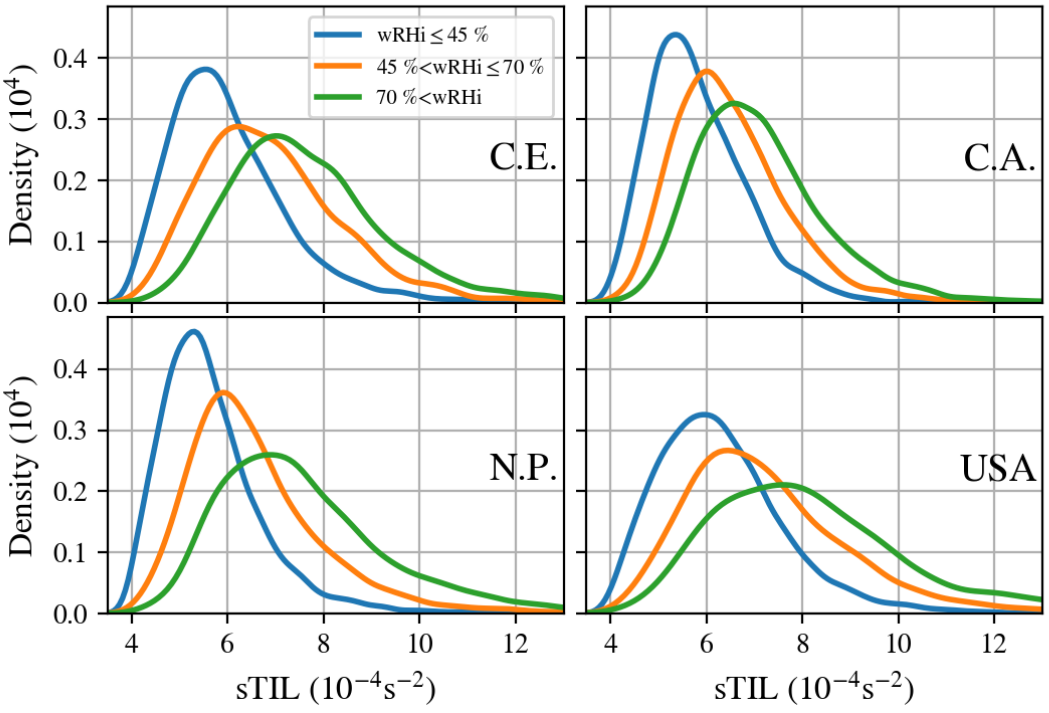

Figure 10. The probability density function of the TIL strength sTIL for average relative humidity categories. Central Europe C.E. (upper left), central Asia C.A. (upper right), the Northern Pacific N.P. (lower left) and the central USA (lower right).

when the average relative humidity with respect to ice is also high for the other regions. Also, the variability of sTIL is increasing with increased humidity in all regions. However, it is visible that the different regions exhibit different distribution shapes of the TIL strength. For example the central USA is showing the highest variability of the sTIL and the highest probability of strong sTIL events. On the contrary central Asia is showing the lowest variability and the lowest probability of strong sTIL events.

To summarize, it can be stated that the influence of humidity on the strength of the TIL is a robust feature of the extratropics. The higher the averaged humidity is, the stronger is the resulting TIL.

3.4 Seasonal variations

This section is covering the seasonal variation of the tropopause inversion layer, which is also covered by the literature, finding that the effect of water vapour on the static stability in the UTLS region to act on seasonal time scales (Kunz et al., 2009; Hegglin et al., 2009).

https://doi.org/10.5194/egusphere-2023-2440
Preprint. Discussion started: 21 November 2023

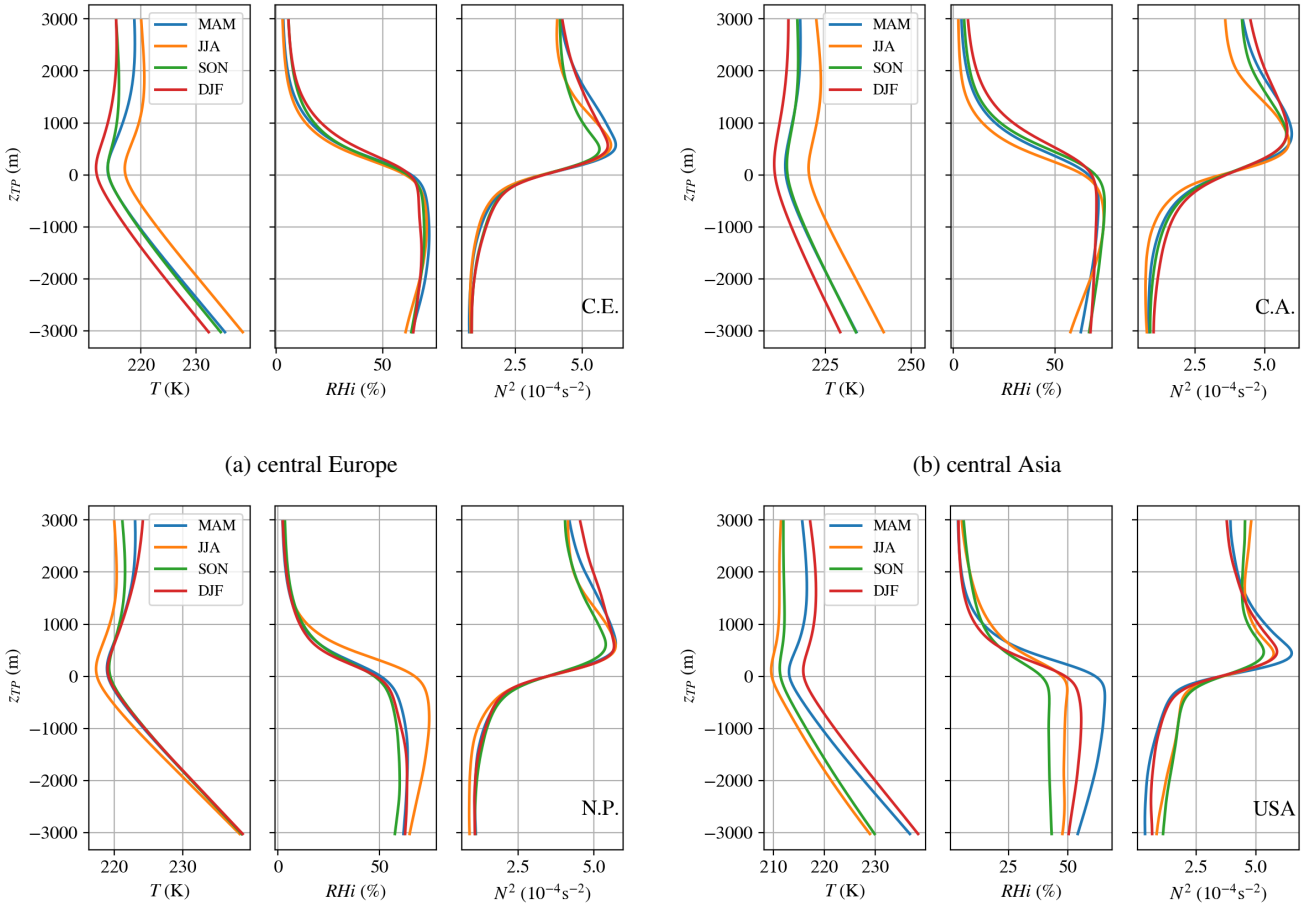

(a) central Europe

(b) central Asia

(c) Northern Pacific

(d) central USA

Figure 11. Mean vertical profiles of temperature T, relative humidity over ice RHi and static stability N^2 in the tropopause relative height z_{TP}. Colors indicate the different seasons, i.e., spring months (MAM) in blue, summer months (JJA) in orange, autumn months (SON) in green, and winter months (DJF) in red.

3.4.1 Seasonal mean vertical profiles

Starting with the temperature profile for central Europe (Fig. 11a) the highest temperatures in the stratosphere and troposphere are found in the summer months; similarly the lowest temperatures are found in the winter months. The autumn and spring months show similar temperatures in the troposphere and at tropopause level, but significantly differ in the stratosphere with autumn temperatures being colder than spring temperatures. For higher levels, the autumn temperatures match the winter temperatures.

https://doi.org/10.5194/egusphere-2023-2440
Preprint. Discussion started: 21 November 2023

The RHi for central Europe on average show little seasonal difference in the troposphere. The most pronounced seasonal differences are found in the first kilometer above the tropopause. Based on the previous findings, it is expected that the spring and summer months show the strongest TIL (high sTIL values) and the thinnest TIL (low dTIL values).

The static stability profiles show a peak of high static stability above the tropopause of similar magnitude $N^2 = 6 \cdot 10^{-4}$ s^{-1} across every season, with a significant difference in static stability above the peak between seasons, confirming previous findings by Schmidt et al. (2010) for the extratropic region (40 °N - 60 °N).

The vertical profiles over central Asia (C.A.) (Fig. 11b) show weak seasonal differences for RHi and the static stability. The summer and autumn months show slightly higher RHi below the tropopause. In contrast the temperature profiles show a high variability throughout the year with the highest temperatures in summer, the lowest temperature in winter.

The Northern Pacific region shows small or even no differences in the temperature and RHi profiles between spring, autumn and winter (Fig. 11c). However, the summer seasonis clearly different, the temperature profile is significantly colder in the tropopause region. At the same time, there is a strong increase in RHi above 2 km below the tropopause. This is supporting the idea that water vapour in the UTLS region has a cooling effect on the tropopause region (Randel et al., 2007; Randel and Wu, 2010). The static stability profile shows little seasonal differences, only the autumn months have a smaller static stability peak.

The central USA region shows the strongest seasonal differences in RHi and N^2. The RHi at the tropopause level takes on the highest values in spring followed by winter, summer and autumn in decreasing order. The peaks of N^2 show the similar pattern with spring exhibiting the strongest peak followed by winter, summer and autumn, respectively. The temperature profile is also different compared to the other regions, with summer exhibiting the lowest and winter the highest temperatures relative to the tropopause. The stronger seasonal differences could be due to lower latitude (42.25 °N instead of 49.75 °N) which was performed to include a region of frequent deep convection in the extratropics.

3.4.2 Seasonal cycle of TIL strength

The correlation between TIL strength and relative humidity is split seasonally using the PDF for different moisture classes for all four regions. The same moisture classes using the average relative humidity with respect to ice (wRHi) as in Fig. 8 are used. The correlation of higher TIL strength (sTIL) values with higher averaged values of wRHi is consistent across every season and every geographical location. Furthermore the correlation of higher sTIL variances with higher wRHi is also present in every region. Also, a distinct feature independent of the geographical region or season is that the low wRHi category shows a mode between $5 \cdot 10^{-4}$ s^{-1} and $6 \cdot 10^{-4}$ s^{-1} with a very low occurrence probability above $8 \cdot 10^{-4}$ s^{-1}.

The region over Central Europe and Central USA show a similar seasonal behaviour. The highest values of sTIL (i.e. "strongest TIL") are found in the spring months, while the minima are found in autumn. The winter months show higher variance and stronger extremes compared to summer, which show on average similar sTIL values as in winter. The winter/summer similarity further support the idea that radiative and baroclinic forcing can have similar amplifying effects. The main difference between central Europe and USA is the considerably higher variance of sTIL in the USA region. Looking at the cyclonic frequencies, the USA region shows a higher frequency than the central Europe across every season. Higher frequency alone

https://doi.org/10.5194/egusphere-2023-2440
Preprint. Discussion started: 21 November 2023

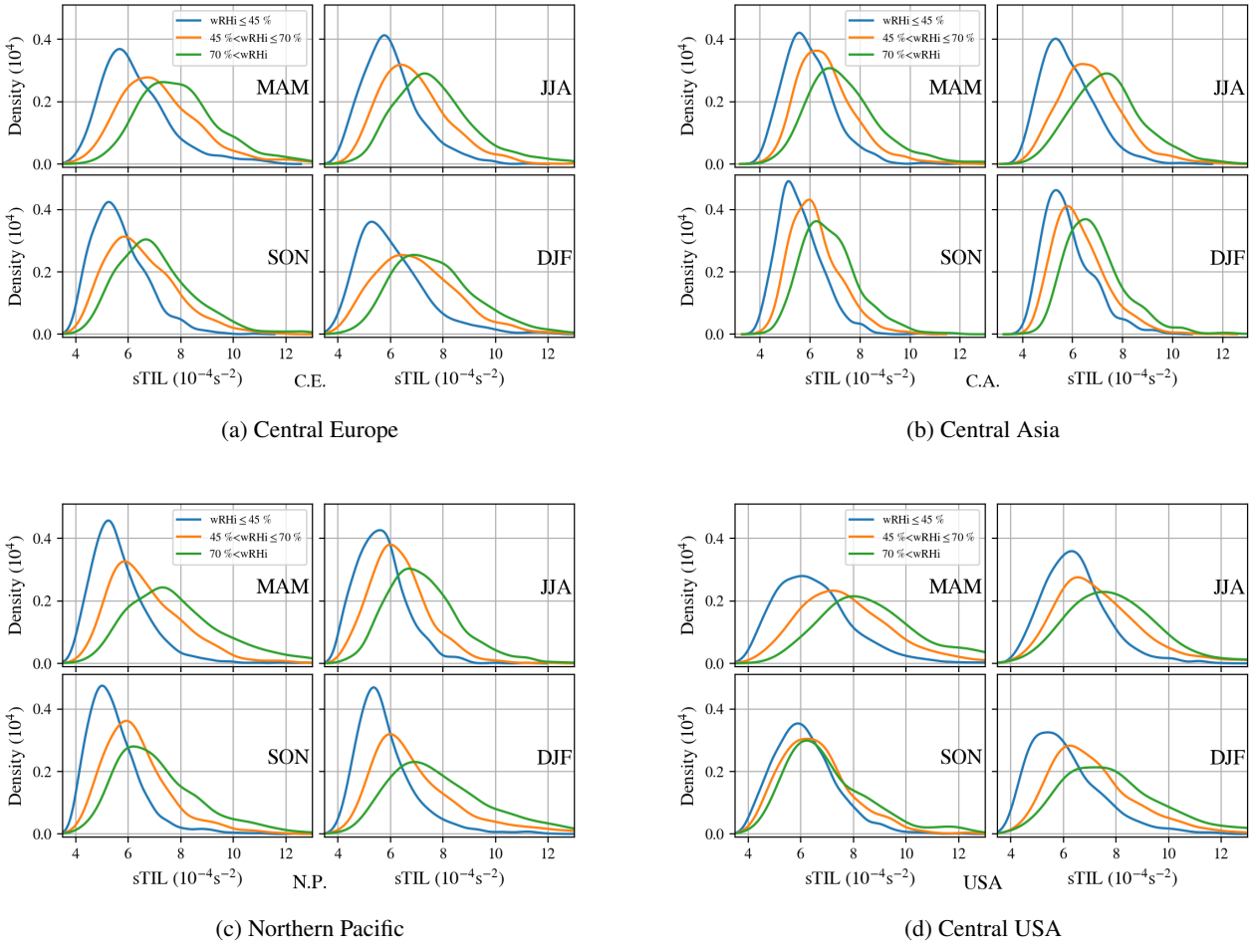

(a) Central Europe

(b) Central Asia

(c) Northern Pacific

(d) Central USA

Figure 12. Seasonal probability density distributions of the tropopause inversion layer strength sTIL for categories of average relative humidity over ice wRHi. Colors indicate the different categories. blue: low category (wRHi $\leq$ 45 %), orange: tmedium category (45 % < wRHi $\leq$ 70 %), green: high category (70 % < wRHi). The panels represent the behaviour for different resions, i.e., results for Central Europe are shown in (a), for Central Asia in (b), Northern Pacific in (c) and Central USA in (d). In addition, in each subfigure the season is indicated, i.e., spring months (MAM), summer months (JJA), autumn months (SON), and winter months (DJF).

does not explain the high variance as the North Pacific with the highest cyclonic frequency do not show higher variance in sTIL. This needs further research in the causes and the forcing mechanisms of the tropopause inversion layer.

The lowest variance of sTIL are found in central Asia (Fig. 12b) across each season and humidity category. Wirth and Szabo (2007) suggested a strengthening of the TIL by baroclinic waves. The baroclinic waves are rare in central Asia as deduced from the low cyclonic frequency, which could explain weaker sTIL values compered to the other region, where baroclinic waves occur more frequently. Also, in Central Asia the highest sTIL values are found in the summer months, which is more

https://doi.org/10.5194/egusphere-2023-2440
Preprint. Discussion started: 21 November 2023

characteristic of the polar TIL as demonstrated by Randel et al. (2007) and Grise et al. (2010). This maximum in sTIL in summer observation supports the radiative mechanism suggested by Randel et al. (2007), since the forcing mechanism by baroclinic waves is reduced to a minimum for this region

The region over the Northern Pacific (Fig. 12c) shows a maximum in the winter and spring months, and a similar minimum in autumn and summer. The maxima are most likely due the baroclinic wave activity, which has its maximum in spring and winter. It is noticeable that the mode in the wettest wRHi category is at higher sTIL values in spring than in winter. This is suggesting that water vapour and its radiative forcing is amplifying the sTIL in spring. The comparison between autumn and summer also shows an interesting aspect. The cyclonic activity has a significant minimum in summer and is lower in autumn than in spring and winter, nonetheless spring and summer are exhibiting similar sTIL values. This gives the indication that the forcing mechanism through baroclinic waves and through the radiative effects might have a similar amplitude.

Overall, consideration of seasonal and geographic differences reveals the overall robust relationship between the strength of TIL and mean moisture in the upper troposphere. However, if one looks more closely at the seasonal cycle in different regions with different synoptic characteristics, one finds different processes seen over the year. At the same time evidence for different formation mechanisms for TIL (radiative forcing, baroclinic waves) can be found.

4 Conclusions

Here we investigated the relationship between various properties of the TIL and relative humidity in the upper troposphere. The example of the long-term series of radiosonde measurements at the Idar-Oberstein station of the German Weather Service clearly showed that the strength of the TIL is strongly related to the relative humidity in the upper troposphere. This can be seen not only in the spatially high-resolution measurement data, but also in the reanalysis data from ERA5 at the same location. The interpolated values reflect the radiosonde's perspective very well, with the expected reductions in the signal due to the coarser spatial resolution of the reanalysis data, such as the weaker representation of gradients in ERA5.

The comparison of the meteorological variables temperature T, relative humidity over ice RHi and static stability N^2 showed that the average difference of a single profile between ERA5 and radiosondes are small. In more detail it was found that the reanalysis data shows on average slightly warmer temperatures in the upper troposphere ($0.034\,\mathrm{K}$). In the lower stratosphere this deviation is slightly higher ($0.121\,\mathrm{K}$). Nevertheless, the comparison shows that the reanalysis data can be used for this kind of investigations very well. Regarding the relative humidity, one can see that the model data is slightly moister (approx. $1.2\,\%\,\mathrm{RHi}$) compared to the radiosondes. The static stability profiles show a too stable behaviour in the UT and a too unstable behaviour in the LS. This difference arises through the coarser resolution of ERA5 which leads to lower absolute values in static stability and weaker gradients in static stability when compared to the radiosondes.

The TIL strength sTIL is considerably weaker in ERA5 then in the radiosonde data, also the variance increases with stronger sTIL. It shows a strong linear correlation, which makes the sTIL a good measure of the tropopause inversion layer to compare across reanalysis and measurement data.

https://doi.org/10.5194/egusphere-2023-2440
Preprint. Discussion started: 21 November 2023

It could be shown that there is a strong positive correlation between the TIL strength sTIL and the average relative humidity with respect to ice wRHi, meaning that higher sTIL are correlated with higher wRHi. It also could be shown that the variance of sTIL increases with higher wRHi. These findings are found in the ERA5 and in the radiosondes data set. Additionally, the TIL depth dTIL shows a negative correlation with wRHi, meaning that that thinner TILs are correlated with higher wRHi.

Extending the analysis with ERA5 to other geographical regions at approximately the same latitude (between 42° and 50° N, Central USA, Central Asia and Northern Pacific) showed that the overall correlation are independent of the region and season. The regional and seasonal analysis also allowed to confirm that the two suggested forcing mechanisms, the dynamical forcing by Wirth and Szabo (2007) and the radiative forcing by Randel et al. (2007) are present. For central Europe, the central USA and the Northern Pacific, sTIL showed is maximum in the seasons of highest cyclonic frequency, this is supporting the dynamical forcing. Central Asia, which is unaffected by cyclonic activity, shows its maximum of sTIL in summer and its minimum in winter and thus supporting the radiative forcing mechanism.

Code availability. The python code for the data evaluation is available upon request.

Data availability. The radiosonde data are publicly available from https://opendata.dwd.de/ at DWD. The ERA5 reanalysis data are publicly available from https://cds.climate.copernicus.eu at ECMWF

Author contributions. DK, PR and PS designed the study; DK carried out the data analyses; DK, PR, and PS contributed to interpreting the results and writing the paper.

Competing interests. The contact author has declared that none of the authors has any competing interests.

Disclaimer. Publisher's note: Copernicus Publications remains neutral with regard to jurisdictional claims in published maps and institutional affiliations.

Acknowledgements. We thank Deutscher Wetterdienst (DWD) for providing the high resolution radiosonde data, and the European Centre for Medium-Range Weather Forecasting (ECMWF) for providing the ERA5 reanalysis data. We thank Daniel Kunkel for getting the data from ECMWF. Philipp Reutter acknowledges support by the DFG within the Transregional Collaborative Research Centre TRR301 TPChange, project C1. Peter Spichtinger acknowledges support by the DFG within the Transregional Collaborative Research Centre TRR301 TPChange,

https://doi.org/10.5194/egusphere-2023-2440
Preprint. Discussion started: 21 November 2023

project B7. The study contributes to the project "Big Data in Atmospheric Physics (BINARY)", funded by the Carl Zeiss Foundation (grant P2018-02-003)

https://doi.org/10.5194/egusphere-2023-2440
Preprint. Discussion started: 21 November 2023

References

Baumgartner, M., Weigel, R., Harvey, A. H., Plöger, F., Achatz, U., and Spichtinger, P.: Reappraising the appropriate calculation of a common meteorological quantity: potential temperature, Atmospheric Chemistry and Physics, 20, 15 585–15 616, https://doi.org/10.5194/acp-20-15585-2020, 2020.

Birner, T.: Fine-scale structure of the extratropical tropopause region, Journal of geophysical research, 111, https://doi.org/10.1029/2005JD006301, 2006.

Birner, T., Dörnbrack, A., and Schumann, U.: How sharp is the tropopause at midlatitudes?, Geophysical Research Letters, 29, https://doi.org/10.1029/2002GL015142, 2002.

Durran, D. R. and Klemp, J. B.: On the Effects of Moisture on the Brunt-Väisälä Frequency, Journal of the atmospheric sciences, 39, https://doi.org/h10.1175/1520-0469(1982)039, 1982.

ECMWF: https://confluence.ecmwf.int/display/CKB/ERA5%3A+data+documentation, 2020.

Erler, A. R. and Wirth, V.: The Static Stability of the Tropopause Region in Adiabatic Baroclinic Life Cycle Experiments, Journal of the atmospheric sciences, 68, https://doi.org/10.1175/2010JAS3694.1, 2011.

Gettelman, A. and Wang, T.: Structural diagnostics of the tropopause inversion layer and its evolution, Journal of geophysical research, 120, https://doi.org/10.1002/2014JD021846, 2015.

Gettelman, A., Hoor, P., Pan, L. L., Randel, W. J., Hegglin, M. I., and Birner, T.: The Extratropical Upper Troposphere and Lower Stratosphere, Reviews of Geophysics, 49, https://doi.org/10.1029/2011RG000355, 2011.

Grise, K. M., J., T. D. W., and Birner, T.: A Global Survey of Static Stability in the Stratosphere and Upper Troposphere, Journal of Climate, https://doi.org/10.1175/2009JCLI3369.1, 2010.

Hantel, M.: Einführung Theoretische Meteorologie, vol. 1, Springer Spektrum, Springer-Verlag Berlin Heidelberg, 1 edn., https://doi.org/10.1007/978-3-8274-3056-4, 2013.

Hegglin, M. I., Boone, C., Manney, G. L., and Walker, K. A.: A global view of the extratropical tropopause transition layer from Atmospheric Chemistry Experiment Fourier Transform Spectrometer O3, H2O, and CO, Journal of Geophysical Research Atmospheres, 114, https://doi.org/10.1029/2008JD009984, 2009.

Hersbach, H., Bell, B., Berrisford, P., Hirahara, S., Horányi, A., Muñoz-Sabater, J., Nicolas, J., Peubey, C., Radu, R., Schepers, D., Simmons, A., Soci, C., Abdalla, S., Abellan, X., Balsamo, G., Bechtold, P., Biavati, G., Bidlot, J., Bonavita, M., Chiara, G., Dahlgren, P., Dee, D., Diamantakis, M., Dragani, R., Flemming, J., Forbes, R., Fuentes, M., Geer, A., Haimberger, L., Healy, S., Hogan, R. J., Hólm, E., Janisková, M., Keeley, S., Laloyaux, P., Lopez, P., Lupu, C., Radnoti, G., Rosnay, P., Rozum, I., Vamborg, F., Villaume, S., and Thépaut, J.: The ERA5 global reanalysis, Quarterly Journal of the Royal Meteorological Society, 146, 1999–2049, https://doi.org/10.1002/qj.3803, 2020.

Hoskins, B. J. and James, I. N.: Fluid Dynamics of the Midlatitude Atmosphere, Wiley, 1 edn., https://doi.org/10.1002/9781118526002, 2014.

Kunz, A., Konopka, P., Müller, R., Pan, L. L., Schiller, C., and Rohrer, F.: High static stability in the mixing layer above the extratropical tropopause, Journal of Geophysical Research Atmospheres, 114, https://doi.org/10.1029/2009JD011840, 2009.

Miloshevich, L. M., Paukkunen, A., Vömel, H., and Oltmans, S. J.: Development and Validation of a Time-Lag Correction for Vaisala Radiosonde Humidity Measurements, Journal of Atmospheric and Oceanic Technology, 21, https://doi.org/10.1175/1520-0426(2004)021, 2004.

https://doi.org/10.5194/egusphere-2023-2440
Preprint. Discussion started: 21 November 2023

Miloshevich, L. M., Vömel, H., Whiteman, D. N., and Leblanc, T.: Accuracy assessment and correction of Vaisala RS92 radiosonde water vapor measurements, Journal of Geophysical Research Atmospheres, 114, https://doi.org/10.1029/2008JD011565, 2009.

Murphy, D. M. and Koop, T.: Review of the vapour pressures of ice and supercooled water for atmospheric applications, Quarterly Journal of the Royal Meteorological Society, 131, 1539–1565, https://doi.org/10.1256/qj.04.94, 2005.

Niebler, S., Miltenberger, A., Schmidt, B., and Spichtinger, P.: Automated detection and classification of synoptic-scale fronts from atmospheric data grids, Weather and Climate Dynamics, 3, 113–137, https://doi.org/10.5194/wcd-3-113-2022, 2022.

Randel, W. J. and Wu, F.: The Polar Summer Tropopause Inversion Layer, Journal of the Atmospheric Sciences, 67, https://doi.org/10.1175/2010JAS3430.1, 2010.

Randel, W. J., Wu, F., and Forster, P.: The Extratropical Tropopause Inversion Layer: Global Observations with GPS Data, and a Radiative Forcing Mechanism, Journal of Atmospheric Sciences, 64, https://doi.org/10.1175/2007JAS2412.1, 2007.

Schmidt, T., Cammas, J.-P., J., S. H. G., Heise, S., Wickert, J., and Haser, A.: Observational characteristics of the tropopause inversion layer derived from CHAMP/GRACE radio occultations and MOZAIC aircraft data, Journal of Geophysical Research Atmospheres, 115, https://doi.org/10.1029/2010JD014284, 2010.

Sonntag, D.: Important new values of the physical constants of 1986, vapour pressure formulations based on the ITS-90, and psychrometer formulae, Zeitschrift für Meteorologie, 40, 1990.

Vaisala: https://www.bodc.ac.uk/data/documents/nodb/pdf/RS92SGP-Datasheet-B210358EN-F-LOW.pdf, 2013.

Vaisala: https://www.vaisala.com/sites/default/files/documents/RS-Comparison-White-Paper-B211317EN.pdf, 2014.

Wernli, H. and Schwierz, C.: Surface Cyclones in the ERA-40 Dataset (1958–2001). Part I: Novel Identification Method and Global Climatology, Journal of the Atmospheric Sciences, 63, https://doi.org/10.1175/JAS3766.1, 2006.

Wirth, V. and Szabo, T.: Sharpness of the extratropical tropopause in baroclinic life cycle experiments, Geophysical Research Letters, 34, https://doi.org/10.1029/2006GL028369, 2007.

WMO: Meteorology—A three-dimensional science: Second session of the commission for aerology, WMO Bulletin, 1957.